Communication: Kinetics of chemical ordering in Ag-Au and Ag-Ni nanoalloys

Florent Calvo, A. Fortunelli, F. Negreiros, D. Wales

Communication: Kinetics of chemical ordering in Ag-Au and Ag-Ni nanoalloys

Cite as: J. Chem. Phys. **139**, 111102 (2013); https://doi.org/10.1063/1.4821582
Submitted: 25 July 2013 . Accepted: 02 September 2013 . Published Online: 17 September 2013

F. Calvo, A. Fortunelli, F. Negreiros, and D. J. Wales

Communication: Kinetics of chemical ordering in Ag-Au and Ag-Ni nanoalloys

F. Calvo,[1,a)] A. Fortunelli,[2] F. Negreiros,[2] and D. J. Wales[3]
[1]*ILM, CNRS UMR 5306 and Université Lyon 1, 43 Bd du 11 Novembre 1918, F69622 Villeurbanne Cedex, France*
[2]*CNR-IPCF, via G. Moruzzi, 1, 56124 Pisa, Italy*
[3]*University Chemical Laboratories, Lensfield Road, Cambridge CB2 1EW, United Kingdom*

(Received 25 July 2013; accepted 2 September 2013; published online 17 September 2013)

The energy landscape and kinetics of medium-sized Ag-Au and Ag-Ni nanoalloy particles are explored via a discrete path sampling approach, focusing on rearrangements connecting regions differing in chemical order. The highly miscible $Ag_{27}Au_{28}$ supports a large number of nearly degenerate icosahedral homotops. The transformation from reverse core-shell to core-shell involves large displacements away from the icosahedron through elementary steps corresponding to surface diffusion and vacancy formation. The immiscible $Ag_{42}Ni_{13}$ naturally forms an asymmetric core-shell structure, and about 10 eV is required to extrude the nickel core to the surface. The corresponding transformation occurs via a long and smooth sequence of surface displacements. For both systems the rearrangement kinetics exhibit Arrhenius behavior. These results are discussed in the light of experimental observations. © *2013 AIP Publishing LLC*. [http://dx.doi.org/10.1063/1.4821582]

Metal nanoparticles containing more than one element (nanoalloys) represent an important and actively investigated subject, owing to their promising novel properties in terms of both basic science and technological applications.[1,2] This interest primarily stems from the wealth of possibilities realized at the structural level when varying a given geometrical framework by distributing the chemical species according to different patterns, thus generating structural homotops.[3] The kinetics of structural rearrangements presents a challenge for computational approaches because of the exponential number of minima that may be dynamically interconnected via sizable energy barriers. Sampling such potential energy landscapes (PELs) is a problem with analogues in other fields, such as protein folding, or the mechanical response of amorphous materials.[4,5]

So far, theoretical studies of chemical rearrangement kinetics in nanoalloys have mostly used molecular dynamics (MD) or accelerated MD (AMD) methods, see, e.g., Refs. 6 and 7. However, these approaches require temperatures close to the melting point in order to speed up the kinetics so that the transformation of interest becomes detectable in a reasonable computational time. As with other biasing methods, it is not clear what effect the bias has on the predictive character of the simulations. In the present work we adopt a different approach that is potentially free of the limitations of MD and AMD methods, where the sampling is achieved via systematic geometry optimization to obtain local minima and the transition states that connect them. To demonstrate the efficiency (millions of minima can be handled) and predictive power, we have applied this procedure to two very different classes of nanoalloys of highly miscible (gold-silver) or fully immiscible (silver-nickel) metals, which represent realistic nanoalloys with contrasting thermodynamic[8] and interesting optical[9,10] properties. A total size of $N = 55$ atoms is chosen, as it represents a "magic number" for gold-silver and falls in the range where clear core and shell regions can be defined. For Ag-Au a composition of around 50:50 is chosen to maximize the complexity of chemical order: $Ag_{27}Au_{28}$. For Ag-Ni, a nickel composition close to 25% is chosen for $Ag_{42}Ni_{13}$ so that particularly stable Ni(core)-Ag(shell) structures can be obtained. We investigate the structural rearrangements involved in the transformation from core-shell structures to either reverse core-shell (Ag-Au), or to Janus-type (Ag-Ni) structures, and characterize the associated kinetics. The variations of the rate constant with temperature exhibit Arrhenius behavior in both cases, but rearrangements proceed according to quite different paths in the two cases. Although they both display large atomic excursions away from the global minimum, rearrangements in $Ag_{27}Au_{28}$ can generally be described in terms of vacancy formation. In contrast, rearrangements in $Ag_{42}Ni_{13}$ exhibit a long and relatively smooth sequence of surface displacements, mostly involving Ag atoms.

To unravel the mechanisms and kinetics for large rearrangements associated with changes in chemical ordering, we use the discrete path sampling (DPS) method,[11,12] which is unbiased and provides access to the rearrangement kinetics from the collected databases through transition state theory for the individual minimum-to-minimum pathways. The present clusters containing 55 atoms support a huge number of stable minima, many of which differ primarily in chemical order.[1,2] Although methods based on an explicit description of electronic structure, especially density functional theory (DFT), could handle such systems,[13] they are not feasible with such a large number of minima and transition states,

a)Electronic mail: florent.calvo@univ-lyon1.fr

unless this number is drastically reduced by assuming a fixed and highly symmetric structural framework.[14] Instead, we adopt a second-moment-approximation (SMA) tight-binding analytic potential, which is reasonably accurate and is commonly used to describe the energetics of nanoalloys.[1,2]

In the case of Ag-Ni, the SMA potential correctly reproduces the complete phase separation of the two metals, with silver surrounding nickel.[15,16] For Ag-Au the parameters favor surface enrichment in Ag due to strain minimization, at variance with more accurate DFT calculations.[17] This deficiency could be solved by including a charge transfer correcting term in the potential, accounting for the electronegativity difference between the two elements.[18] However, at finite temperatures more relevant to the present work, the potential predicts a high miscibility,[8] in agreement with the known solid solution formed in the bulk and nanoscale forms of the Ag-Au mixture.[19] In addition, reverse Au(core)-Ag(shell) configurations can be obtained experimentally by exploiting the higher oxygen affinity of Ag with respect to Au.[20] All the databases of connected minima were built and expanded using the DPS method.[11,12] More details about the computations are provided as the supplementary material.[16]

Gold-silver nanoalloys exhibit a frustrated energy landscape, in which a given structure is associated with a combinatorially large number of homotops differing in their chemical order, with very similar atomic positions. At size 55, the two-layer Mackay icosahedron is the most stable structure, and the lowest part of the PEL consists of different homotops with alternative arrangements of Au and Ag within the icosahedron, as depicted in the disconnectivity graph.[16] Among these low-lying minima, two families of structures can be identified with all 14 core atoms being either gold (core-shell) or silver (reverse core-shell).

Two order parameters were used to describe the transformation from core-shell to reverse core-shell in the $Ag_{27}Au_{28}$ nanoalloy. Radii of gyration appear suitable for distinguishing between the end points, so we define

$$R_g^2 = \frac{1}{N_{\mathrm{Ag}} + N_{\mathrm{Au}}} \sum_{i \in \mathrm{Ag,Au}} r_i^2,$$

$$\text{and} \qquad \Delta R_g^2 = R_{g,\mathrm{Ag}}^2 - R_{g,\mathrm{Au}}^2 = \frac{1}{N_{\mathrm{Ag}}} \sum_{i \in \mathrm{Ag}} r_i^2 - \frac{1}{N_{\mathrm{Au}}} \sum_{i \in \mathrm{Au}} r_i^2 \qquad (1)$$

as the global squared radius of gyration and the squared radius of gyration for silver relative to gold, respectively. Figure 1 shows these order parameters for the 1 017 958 minima in our database plotted as $(R_g^2, \Delta R_g^2)$. This scatter plot clearly shows the most compact icosahedral minima as a series of nearly discrete spots at low R_g^2, differing in ΔR_g^2 by steps corresponding to Ag or Au atoms belonging to different shells. Within this region of low R_g^2, the core-shell and reverse core-shell regions are defined from the extreme values of ΔR_g^2, either with silver outside (high ΔR_g^2) or inside (low ΔR_g^2). The DPS rate calculations used these definitions as the product and reactant states for the transformation. In addition to the core-shell minima, the Janus-type clusters with a side-by-side phase separation appear around $\Delta R_g^2 \sim 0$.

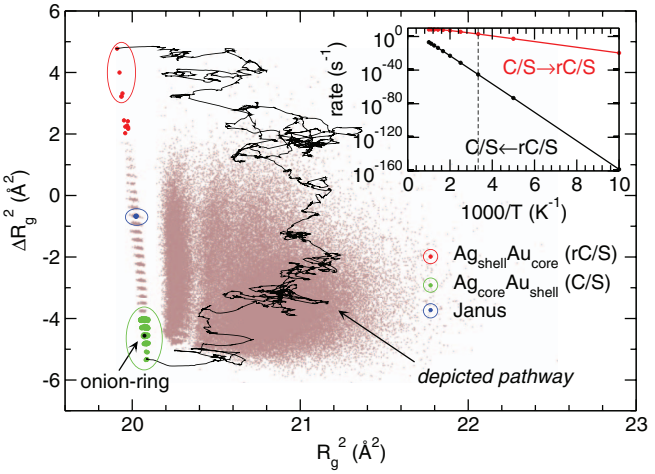

FIG. 1. Scatter plot of the squared radius of gyration ΔR_g^2 for silver relative to gold, versus the global squared radius of gyration R_g^2, for the database of local minima of $Ag_{27}Au_{28}$. The core-shell (reverse core-shell) regions where the 14 core atoms are pure silver (pure gold) are highlighted in green and red, respectively, as well as a Janus-type configuration in which the icosahedron is split into two halves of pure silver and pure gold. A continuous pathway connecting the most stable minima of the core-shell and reverse core-shell regions is depicted. (Inset) The calculated rate constants for the transitions between the core-shell and reverse core-shell regions as Arrhenius plots.

Most of the map in Fig. 1 is filled with defective ($R_g^2 \sim 20.2$–20.4 Å^2), or even non-icosahedral ($R_g^2 > 20.4$ Å^2) minima. A pathway connecting the most stable minima in the core-shell and reverse core-shell regions was obtained using Dijkstra's algorithm,[21] as implemented in the PATHSAMPLE program.[22] This path corresponds to the largest contribution to the rate constant at 300 K when intervening minima are placed in steady state,[12] and its main steps are shown in Fig. 2 as a function of the integrated Euclidean distance along the sequence of minimum-saddle-minimum. The rearrangement proceeds in two stages: at the beginning of the

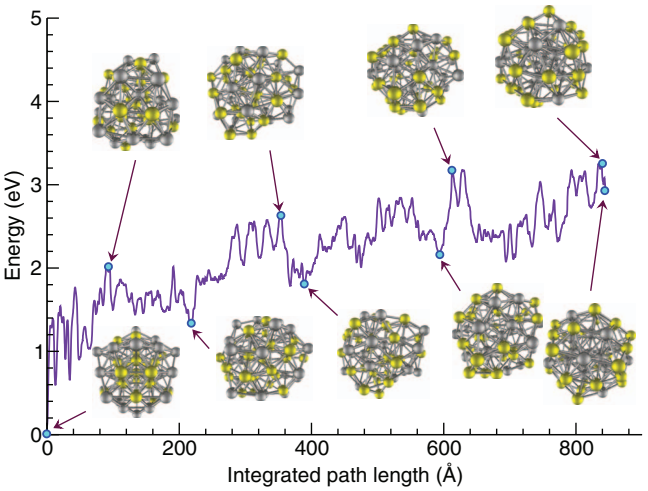

FIG. 2. Pathway transforming the two lowest potential energy structures of the core-shell and reverse core-shell regions for $Ag_{27}Au_{28}$ to each other, also depicted in Fig. 1. Some intervening minima and transition states along the path are highlighted. All energies are relative to the global minimum.

transformation, when many atoms need to move, the cluster breaks the icosahedral symmetry, adding a few atoms in the overlayer, significantly deforming the cluster and increasing its radius (see Fig. S1(a)[16]). The strain from this process is progressively released, especially in the second stage, when vacancies appear from Ag atoms moving to the overlayer and exchanging with Au atoms at the surface, allowing them to diffuse into the core. The number of mixed and homologous bonds stays nearly constant (see Fig. S1(b)[16]) and both Ag and Au atoms undergo substantial excursions (see Fig. S1(c)[16]).

The calculated rate constants for the transformation, shown as an inset in Fig. 1, display essentially Arrhenius behavior, with overall forward and backward activation energies of 2.74 and 0.62 eV for the core-shell↔reverse core-shell transformation. Those values are consistent with the highest barrier heights on the pathway in Fig. 2. At room temperature, only the transformation from the (metastable) core-shell to the (most stable) reverse core-shell regions would be seen for reasonable observation time scales.

In contrast, the Ag-Ni nanoalloy has a strong tendency for phase segregation and a preference for nickel to be surrounded by silver. There is now a high energetic cost associated with alloying, but the difference in interactions destabilizes the two-layer icosahedron in favor of deformed minima, where the nickel core is off-center.[8] The resulting PEL displays a broad variety of core-shell structures with different shapes, belonging to funnels associated with different core geometries, as shown in the disconnectivity graph.[16]

The binding energy and the nickel-specific gyration radius $R^2_{g,\mathrm{Ni}}$ are good order parameters to distinguish the core-shell minima from minima having Janus-type segregated structures. A two-dimensional scatter plot of the order parameters for the 192 300 minima of our database, shown in Fig. 3, highlights the two states considered in transformations, where the nickel core is extruded from the nanoalloy center (core-shell) and finishes in a Janus structure. Because the Janus minima span a broad energetic and structural range, a specific Janus minimum based on icosahedral packing was selected to illustrate the complex rearrangement of this extrusion transformation. This icosahedral minimum lies quite high in energy (about 10 eV above the global minimum), and is connected to the core-shell minima by a longer and smoother sequence of surface displacements, as shown in Fig. 4. Here the Ni atoms mostly remain in an identifiable subcluster, while changing their shape from a thin surface layer to a cluster inside the core: phase separation is essentially conserved during the whole process. Concurrently, the Ag atoms at the surface progressively cover the Ni aggregate, while the number of mixed bonds increases linearly at the expense of homologous bonds (see Fig. S2(b)[16]) and R^2_g for the complete cluster decreases (see Fig. S2(a)[16]). In this surface-dominated transformation Ag atoms undergo much larger excursions than Ni atoms (see Fig. S2(c) in the supplementary material[16]) and the role of vacancies is minor, in contrast to the Ag-Au case.

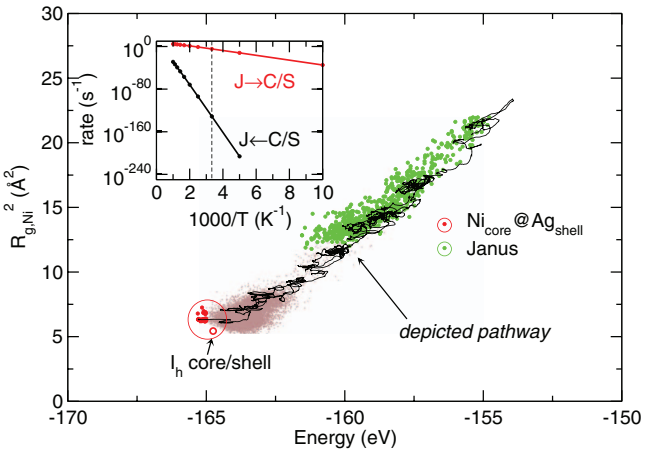

FIG. 3. Squared gyration radius $R^2_{g,\mathrm{Ni}}$ for nickel versus binding energy in the database of local minima of $Ag_{42}Ni_{13}$. The core-shell and Janus regions in which the nickel component is surrounded or next to the silver component are highlighted in red and green, respectively. A continuous pathway connecting the (core-shell) global minimum to a Janus minimum based on icosahedral packing is depicted. (Inset) The calculated rate constants for the transitions between the two core-shell and Janus regions in Arrhenius plots.

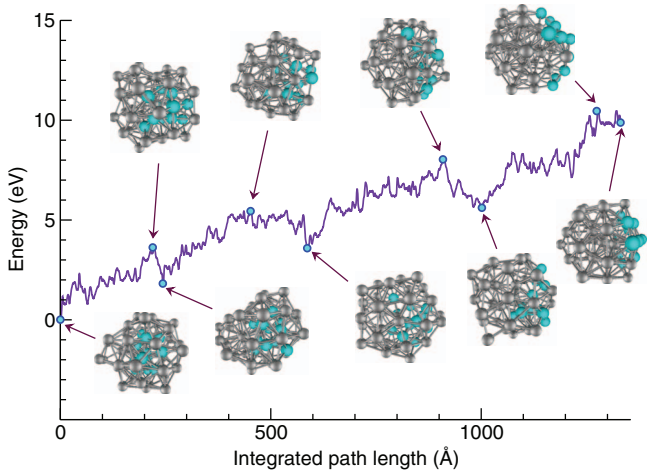

FIG. 4. Pathway transforming the core-shell global minimum of $Ag_{42}Ni_{13}$ to a icosahedral Janus-type minimum, also depicted in Fig. 3. Some intervening minima and transition states along the path are highlighted. All energies are relative to the global minimum.

The rate constants associated with the extrusion rearrangement, obtained from the DPS analysis, again exhibit Arrhenius behavior (see inset of Fig. 3) with activation energies of 8.80 and 0.87 eV for the core-shell→Janus and Janus→core-shell transformations, respectively. On average, the kinetics are slower for Ag-Ni with respect to Ag-Au: this difference is related to the presence of stronger Ag-Ni bonds that limit the structural freedom of the system.

The fivefold symmetric, randomly alloyed structures obtained for Ag-Au nanoparticles are consistent with previous observations,[20] even though more complex arrangements[23] can also be produced. Accurate experimental data relevant to the present work only exist for much larger nanoparticles,[24,25] which often exhibit crystalline morphologies,[26] different from the present icosahedral-based structures. A systematic analysis of particles of this size would require a great deal more computer time; comparison of the present results with available experiments already provides significant new insight. Our results for $Ag_{27}Au_{28}$ are consistent with the experimental

observation of enhanced interdiffusion due to structural freedom at the surface of Ag-Au nanoparticles.[27] In particular, the formation of defects such as vacancies at the bimetallic interface can also be seen in our simulations, although surface diffusion processes with lower energy barriers definitely prevail. 8 nm Au(core)-Ag(shell) particles were recently transformed into randomly alloyed particles over about 2 h at 250 °C,[25] while in a previous experiment 24 h at 100 °C were needed to interconvert Ag(core)-Au(shell) 15 nm particles into random alloys.[24] From our simulations we estimate that the alloying process for a 55-atom Ag-Au cluster should be complete in about 0.1 s at 250 °C. Assuming that the total alloying time scales as $N^{5/3} \div N^2$, with N the number of atoms in the particle, we estimate 0.5–5.0 h as the time scale needed for spontaneously alloying a 8 nm particle. Given that nanoparticles are larger in the experiment,[25] our predictions for the transformation rates thus lie within the observed range. It is noteworthy that the DPS approach can provide estimates of experimental time scales far beyond the reach of standard molecular dynamics.

Ag-Ni nanoparticles can be synthesized as solid solutions or random alloys[28] or even Ag(core)-Ni(shell) particles[29] but only as metastable, kinetically trapped configurations,[30] which evolve upon annealing into the thermodynamically preferred Ni(core)-Ag(shell) structure.[15,31] It was found that 2–5 nm particles synthesized in the gas phase do indeed exhibit Ni(core)-Ag(shell) arrangements.[8–10] However, the conditions of these experiments make it difficult to determine the equivalent growth kinetic parameters, preventing a direct comparison with our prediction that Ag-Ni particles alloy more slowly than Ag-Au particles.

In summary, we have shown how a thorough investigation of the chemical ordering kinetics in nanoalloys is computationally feasible using state-of-the-art methodology combined with analytic interatomic potentials. Application of discrete path sampling[11,12] to two prototypical systems with contrasting miscibility properties (random mixing or core-shell segregation) shows how compositional rearrangement proceeds via rather diverse atomistic mechanisms (and different rates) in the two systems, which also exist in homogeneous clusters,[32] and range from vacancy formation to surface diffusion. The predicted interconversion rates are of the order of seconds to hundreds of seconds, in agreement with experimental estimates for larger crystalline nanoparticles,[24,25] confirming an enhancement of the kinetics of interdiffusion in nanosystems with respect to the bulk.[27]

F.C. acknowledges generous computational resources from the regional Pôle Scientifique de Modélisation Numérique in Lyon. Financial support from the ERC-AG SEPON project and networking from the COST Action MP0903 "Nanoalloys" are gratefully acknowledged.

[1] *Nanoalloys: From Fundamentals to Emergent Applications*, edited by F. Calvo (Elsevier, Amsterdam, 2013).
[2] *Metal Clusters and Nanoalloys: From Modeling to Applications*, edited by M. M. Mariscal, O. A. Oviedo, and E. P. M. Leiva (Springer, Berlin, 2013).
[3] J. Jellinek and E. B. Krissinel, Chem. Phys. Lett. **258**, 283 (1996).
[4] D. J. Wales, *Energy Landscapes* (Cambridge University Press, Cambridge, 2003).
[5] J. Marian, B. D. Wirth, A. Caro, B. Sadigh, G. R. Odette, J. M. Perlado, and T. Diaz de la Rubia, Phys. Rev. B **65**, 144102 (2002).
[6] A. F. Voter, F. Montalenti, and T. C. Germann, Annu. Rev. Mater. Res. **32**, 321 (2002).
[7] T. Niiyama, S.-I. Sawada, K. S. Ikeda, and Y. Shimizu, Chem. Phys. Lett. **503**, 252 (2011).
[8] F. Calvo, E. Cottancin, and M. Broyer, Phys. Rev. B **77**, 121406(R) (2008).
[9] E. Cottancin, M. Gaudry, M. Pellarin, J. Lermé, L. Arnaud, J.-R. Huntzinger, J.-L. Vialle, M. Treilleux, P. Mélinon, J.-L. Rousset, and M. Broyer, Eur. Phys. J. D **24**, 111 (2003).
[10] M. Gaudry, E. Cottancin, M. Pellarin, J. Lermé, L. Arnaud, J.-R. Huntzinger, J.-L. Vialle, M. Broyer, J.-L. Rousset, M. Treilleux, and P. Mélinon, Phys. Rev. B **67**, 155409 (2003).
[11] D. J. Wales, Mol. Phys. **100**, 3285 (2002); **102**, 891 (2004).
[12] D. J. Wales, Int. Rev. Phys. Chem. **25**, 237 (2006).
[13] R. Ferrando, A. Fortunelli, and R. L. Johnston, Phys. Chem. Chem. Phys. **10**, 640 (2008).
[14] F. R. Negreiros, F. Taherkhani, G. Parsafar, A. Caro, and A. Fortunelli, J. Chem. Phys. **137**, 194302 (2012).
[15] G. Rossi, A. Rapallo, C. Mottet, A. Fortunelli, F. Baletto, and R. Ferrando, Phys. Rev. Lett. **93**, 105503 (2004).
[16] See supplementary material at http://dx.doi.org/10.1063/1.4821582 for the disconnectivity graphs of the two clusters, the details and parameters of the potential, and additional properties of the two rearrangement pathways. Animations of these two rearrangements are also provided.
[17] V. Bonačić-Koutecký, J. Burda, R. Mitrić, M. Ge, G. Zampella, and P. Fantucci, J. Chem. Phys. **117**, 3120 (2002); L. O. Paz-Borbon, R. L. Johnston, G. Barcaro, and A. Fortunelli, *ibid.* **128**, 134517 (2008); L.-L. Wang, T. L. Tan, and D. D. Johnson, Phys. Rev. B **86**, 035438 (2012).
[18] M. Cerbelaud, R. Ferrando, G. Barcaro, and A. Fortunelli, Phys. Chem. Chem. Phys. **13**, 10232 (2011).
[19] T. B. Massalski, J. L. Murray, L. J. Bernett, and H. Baker, *Binary Alloy Phase Diagrams* (American Society for Metals, Metals Park, OH, 1986), Vol. 1.
[20] D. Belić, R. L. Chantry, Z. Y. Li, and S. A. Brown, Appl. Phys. Lett. **99**, 171914 (2011).
[21] E. W. Dijkstra, Numer. Math. **1**, 269 (1959).
[22] D. J. Wales, *PATHSAMPLE: A program for generating connected stationary point databases and extracting global kinetics*, see http://www-wales.ch.cam.ac.uk/software.html.
[23] D. A. Ferrer, L. A. Diaz-Torres, S. Wua, and M. Jose-Yacaman, Catal. Today **147**, 211 (2009); A. Mayoral, A. Vazquez-Duran, D. A. Ferrer, J. M. Montejano-Carrizales, and M. Jose-Yacaman, Cryst. Eng. Comm. **12**, 1090 (2010).
[24] C. Wang, S. Peng, R. Chan, and S. Sun, Small **5**, 567 (2009).
[25] M. S. Shore, J. Wang, A. C. Johnston-Peck, A. L. Oldenburg, and J. B. Tracy, Small **7**, 230 (2011).
[26] W. G. Menezes, V. Zielasek, G. I. Dzhardimalieva, S. I. Pomogailo, K. Thiel, D. Wohrle, A. Hartwig, and M. Baumer, Nanoscale **4**, 1658 (2012).
[27] T. Shibata, B. A. Bunker, Z. Zhang, D. Meisel, C. F. Vardeman II, and J. D. Gezelteer, J. Am. Chem. Soc. **124**, 11989 (2002).
[28] Z. Zhang, T. M. Nenoff, K. Leung, S. R. Ferreira, J. Y. Huang, D. T. Berry, P. P. Provencio, and R. Stumpf, J. Phys. Chem. C **114**, 14309 (2010); C. Srivastava, S. Chithra, K. D. Malviya, S. K. Sinha, and K. Chattopadhyay, Acta Mater. **59**, 6501 (2011).
[29] M. Tsuji, S. Hikino, M. Matsunaga, Y. Sano, T. Hashizume, and H. Kawazumi, Mat. Lett. **64**, 1793 (2010); L. Xia, X. Hua, X. Kanga, H. Zhao, M. Sun, and X. Cihen, Colloids Surf., A **367**, 96 (2010).
[30] C. Srivastava, Mater. Lett. **70**, 122 (2012); B. M. Mundotiya and C. Srivastava, Electrochem. Solid-State Lett. **15**, K41 (2012).
[31] M. Molayem, V. G. Grigoryan, and M. Springborg, J. Phys. Chem. C **115**, 7179 (2011).
[32] D. J. Wales and L. J. Munro, J. Phys. Chem. **100**, 2053 (1996).